SAND2000-3208J

DOUBLE-DIFFUSIVE FINGER CONVECTION: FLOW FIELD EVOLUTION IN A HELE-SHAW CELL

Clay A. Cooper
Desert Research Institute
2215 Raggio Parkway
Reno, Nevada 89512
775.673.7372; clay@dri.edu

Robert J. Glass
Flow Visualization and Processes Laboratory
Sandia National Laboratories
P.O. Box 5800
Albuquerque, New Mexico 87185-0735

Scott W. Tyler
Department of Environmental and Resource Sciences and
Department of Geological Sciences
University of Nevada, Reno
LMR 267
Reno, Nevada 89557-0180

ABSTRACT

Double-diffusive finger convection is a hydrodynamic instability that can occur when two components with different diffusivities are oppositely stratified with respect to the fluid density gradient as a critical condition is exceeded. Laboratory experiments were designed using sodium chloride and sucrose solutions in a Hele-Shaw cell. A high resolution, full field, light transmission technique was used to study the development of the instability. The initial buoyancy ratio (R_ρ), which is a ratio of fluid density contributions by the two solutes, was varied systematically in the experiments so that the range of parameter space spanned conditions that were nearly stable (R_ρ=2.8) to those that were moderately unstable (R_ρ=1.4). In systems of low R_ρ, fingers develop within several minutes, merge with adjacent fingers, form conduits, and stall before newer-generated fingers travel through the conduits and continue the process. Solute fluxes in low R_ρ systems quickly reach steady state and are on the order of 10^{-6} m^2 sec^{-1}. In the higher R_ρ experiments,

DISCLAIMER

DISCLAIMER

Portions of this document may be illegible in electronic image products. Images are produced from the best available original document.

fingers are slower to evolve and do not interact as dynamically as in the lower R_ρ systems. Our experiment with initial R_ρ=2.8 exhibited flux on the order of that expected for a similar diffusive system (i.e., 10^{-7} m^2 sec^{-1}, although the structures were very different than the pattern of transport expected in a diffusing system. Mass flux decayed as $t^{1/2}$ in two experiments each with initial R_ρ=2.4 and 2.8.

1.0 INTRODUCTION

When multiple density-affecting solutes are dissolved in a buoyantly stable fluid, the different rates of molecular diffusion can result in the development of small-scale structures that lead to an enhanced rate of mass transport. The structures that develop are the result of a hydrodynamic instability; their qualitative and quantitative features are very different than those associated with advective, dispersive, and/or diffusive transport. When the solutes are oppositely stratified, two types of structures can develop. If the slower diffusing solute is stabilizing to the vertical density gradient (i.e., heavy on bottom), double-diffusive oscillations develop as parcels of fluid travel vertically and reverse their buoyancy every half cycle. When the faster diffusing solute is stabilizing to the vertical density gradient, double-diffusive fingers develop that grow in a single vertical direction. In either system, it is diffusion of the component stabilizing to the vertical density gradient that destabilizes the system. For example, in the case of the finger instability, diffusion of the faster diffusing solute allows the release of potential energy of the slower diffusing solute, resulting in convection. Hence, diffusion is both a driver and brake in these systems.

The finger instability was hypothesized to occur in parts of the low- to mid-latitudes of the world's oceans for many years before techniques were developed to detect and confirm its presence in the 1970s. In the ocean, fingers are created as a result of a difference in diffusivities between heat and solute. Water above the thermocline is warmer and saltier than that below, resulting in thermohaline (double-diffusive finger) convection. Thermohaline convection has been shown to be an important control on the balance of heat and salt in the ocean and to drive large-scale circulation where it occurs. Guided by the experience of the oceanographic community of the 1960s, Green (1984), Imhoff and Green (1988), Phillips (1991), and Cooper et al. (1997) have hypothesized the existence of subsurface environments (porous media and fractures) favorable to double-diffusive finger convection. These include environments where multiple dissolved density-affecting components are present: deep circulation in marine and terrestrial alluvial basins; interaction between groundwater

and playas, estuaries and other bodies of surface water; circulation of fluids in metamorphic environments; and transport of dissolved solutes from solid waste landfills.

The behavior of a developing double-diffusive convection system is affected by the magnitude of its deviation from the equilibrium state toward which the system evolves (Turner, 1979). One measure of the degree of disequilibrium in these systems utilizes the nondimensional Rayleigh number of each component, that is

$$Rs_i = \beta_i \Delta c_i g k H / D_i \nu, \tag{1}$$

where β [dimensionless] refers to the "contraction" coefficient for solutes (expansion coefficient for the case where one component is heat), Δc [dimensionless] is the change in concentration of a solute (change in temperature for heat) over some characteristic length H [L], g is the acceleration due to gravity [L t^{-2}], k is the intrinsic permeability [L^2], ν is the kinematic viscosity of the solution [L^2 t^{-1}], D_i is the molecular diffusivity of a component [L^2 t^{-1}], and the subscripts i=1,2 refer to the faster and slower diffusing components, respectively. For the case where one or both of the Rayleigh numbers greatly exceeds a critical condition, there is nearly universal agreement that the buoyancy ratio,

$$R_\rho = \beta_1 \Delta c_1 / \beta_2 \Delta c_2, \tag{2}$$

emerges as the appropriate dimensionless parameter that defines the degree of disequilibrium. Experiments in ordinary fluids (Turner, 1967; Stern and Turner, 1969; Lambert and Demenkow, 1971; Griffiths and Ruddick, 1980; Taylor, 1991; Taylor and Veronis, 1996), porous media (Imhoff and Green, 1988), and Hele-Shaw cells (Cooper et al., 1997) have shown that as R_ρ decreases from the stability boundary at τ^{-1} (approximately 80 and 3 for heat/salt and salt/sucrose systems, respectively), the system transitions from being diffusion-dominated to convection-dominated with increasing mass fluxes and finger velocities. The molecular diffusivity ratio, τ, is defined as $0 < \tau < 1$.

Here we present the results of a unique set of experiments conducted in a Hele-Shaw cell that consider system evolution after the onset of instability for the NaCl (sodium chloride) and sucrose system. These experiments were originally used by Cooper et al. (1997) to explore the theoretical boundary dividing stable double diffusion and unstable double-diffusive convection in a Hele-Shaw cell. While holding the initial Rs_l constant (i.e., salt concentration), R_ρ was varied in the experiments (by adjusting the lower diffusivity sucrose solution) over a range from nearly stable (2.8) to moderately unstable (1.4), yielding system behavior as a function of the initial degree of disequilibrium. Using a quantitative light transmission technique, we tracked the concentration field of a dye added to one of the solutions as a function of time throughout the course of each experiment. This technique is ideal for capturing detailed structure on the sub-mm scale and larger. Such data allow us to describe the dynamics of the evolving unstable flow field as a function of time through characterization of structural measures, such as the height of the finger gradient zone and finger width, as well as mass transfer.

2.0 EXPERIMENTAL DESIGN

Cooper et al. (1997) presented the results of 12 experiments designed to study the location of the stability boundary for a fluid layered with a solution of sucrose over a solution of sodium chloride (NaCl) in a Hele-Shaw cell. The experiments were conducted in a region of Rayleigh parameter space from Rs_1~141,000-145,000 and Rs_2~132,000-288,000, based upon the height of the cell. Rs_1 was selected so that solute concentrations might be representative of environmental contamination problems, while Rs_2 was varied to yield buoyancy ratios from 1.4 (most unstable) to 2.8 (nearly stable). While Cooper et al. (1997) were only concerned with system stability, here we analyze the data set to consider the evolution of the unstable flow field as a function of R_ρ. The results of four of these experiments that span the same range of parameter space as the original 11 unstable experiments are analyzed in detail (Table 1); the remaining seven experiments were used to

confirm qualitative trends. One of the original experiments was stable and thus not considered here.

Low Reynolds number flows in Hele-Shaw cells can mimic two-dimensional flows through porous media (Bear, 1988) and are direct models of flow through smooth-walled fractures. The cell "permeability" is $b^2/12$ where b is the cell gap. Conditions on velocities and convective length scales that must be met for analogy with porous systems were discussed in relation to the data in Cooper et al. (1997). Though these conditions were all satisfied, Hele-Shaw cells are still not always an exact analogue to porous media. However, they allow one to study many fundamentals of viscous flow phenomena that are difficult to analyze with experimental porous media. In our case, the Hele-Shaw cell allowed us to use a quantitative light transmission technique to measure the concentration field of a dye dissolved in one of the solutions, resulting in a temporal sequence of high-resolution concentration images of the entire cell.

2.1 Experimental Apparatus

Experiments were conducted in a transparent Hele-Shaw cell (310 mm tall, 170 mm wide) with a gap between 0.495 and 0.515 mm, depending on the experiment. Impermeable boundaries defined the edges of the cell except for two small regions across the top that allowed air to escape as the cell was filled. The cell was filled from the bottom with a NaCl solution, and a thin plastic slider (0.3 mm thick) was inserted across the cell within a horizontal groove (1.0 mm deep × 0.4 mm wide) that had been milled horizontally across the center of the inside of each plate. The cell was then filled from above with the sucrose solution. The slider was removed to bring the two solutions in contact and begin the experiment. As the slider was removed, a small transition (mixed) zone between the fluids always resulted. Measurements of the height of this zone by Cooper et al. (1997) determined that it varied horizontally across the cell and from experiment to experiment, ranging from 1.1 to 16.4 mm for all experiments (see their Plate 1 for an example image of the initial transition zone).

A light absorbing dye was added to one of the two solutions so that a quantitative light transmission technique using a full-field diffused light source and electronically cooled and shuttered CCD camera (2048 x 2048 pixels, 4096 gray levels) could be applied to measure the two-dimensional concentration field in time. Each pixel measured a 0.18 mm x 0.18 mm region of the cell (this was incorrectly reported in Cooper et al. [1997] as 5.5 pixel mm^{-2}). The concentration of the dye used (0.0005 kg FD&C blue #1/kg water or less) increased the solution density by less than 0.2%. The molecular diffusion coefficient was previously measured to be $5.67 \times 10^{-10} m^2 sec^{-1}$ (Detwiler et al., in press).

2.2 Digital Image Reduction to Quantitative Concentration Fields

Evaluation of our digital image reduction procedure reported in Cooper et al. (1997) led to several improvements. All images were first adjusted to remove small temporal fluctuations in light source using a constant density stepped wedge present in each image. Because the cell was moved between experiments and between each calibration curve image, we then aligned the images by shifting each image using a reference point. Each adjusted and aligned image was then converted to normalized light intensity (I_n) to remove large spatial variations in light transmittance through the cell using the following:

$$I_n = \frac{I_i - I_{cl}}{I_{dye} - I_{cl}} \tag{3}$$

Here I_i is the gray level of an individual pixel in the image being normalized, and I_{dye} and I_{cl} are reference images for the fully dyed ($c = c_o$) and clear ($c = 0$) conditions. Each pixel was then converted to normalized concentration through a calibration curve relating normalized concentration (c/c_o) to I_n. The calibration curve was built by measuring the intensity fields within the cell for a series of dye concentrations. Because of slight differences (<5%) in the average gap in the top and bottom of the cell, a separate calibration curve was built for the top and bottom halves of the cell. The correlation coefficient was greater than 0.99 for both calibration curves. Accuracy of our

method was also checked by tracking the total mass in the cell for every experiment as calculated by taking the concentration image times the Hele-Shaw cell gap field measured using the method of Detwiler et al. (1999) and then summing over all points in the image. Mass was found to be conserved to within 1.5% for all images in all experiments, a slight improvement on the image reduction method discussed in Cooper et al. (1997), where it was reported as 2%. Evaluation of the precision error at a point using approaches similar to Detwiler et al. (1999) and Detwiler et al. (in press) showed the combined error due to temporal fluctuation (single images with no temporal averaging) and alignment shifts (always greater than 1 pixel) to be ~ 4%. Averaging over many points in an image to build concentration profiles or fluxes into regions of the cell yields measures that rapidly decreases the precision based error.

3.0 RESULTS AND DISCUSSION

Each experiment began by removing the slider separating the two solutions in the upper and lower halves of the Hele-Shaw cell. Depending upon the degree of instability, initial perturbations develop either rapidly (low initial R_ρ) or slowly (on the order of several hours for high initial R_ρ), select their own internal length scale, and develop into finite amplitude fingers. Fingers initially develop within the transition zone but eventually grow outside the zone. Figure 1 presents a time series of normalized concentration images for R_ρ=1.4 and 2.8. The images were chosen such that the mean c/c_o in the upper half of the cell is equivalent for respective images in time and chosen to be 0.018, 0.036, and 0.054; the corresponding times for these images are 9, 68, and 146 minutes (R_ρ=1.4) and 370, 2752, and 6871 minutes (R_ρ=2.8). Late-time images for R_ρ=1.4, 1.8, and 2.4 corresponding to times of 320, 1085, and 3398 minutes, respectively, and a common mean c/c_o in the upper half of the cell of 0.10, are shown in Figure 2. A late time image for R_ρ=2.8 is not shown because the experiment was terminated before this concentration was reached. Across Figures 1

and 2, we clearly see R_ρ to influence concentration field structure, finger velocity and time scale. In the following, we first describe the temporal evolution of the concentration fields (section 3.1). We then consider structural measures of the concentration field including concentration profiles, finger gradient zone height and finger width (section 3.2). Finally we analyze the transfer of mass as a function of R_ρ (section 3.3).

3.1 General Description of Evolving Concentration Fields

Animations of the concentration fields taken over the course of each experiment show a rich and complex behavior. For R_ρ=1.4, fingers develop from a region straddling the initial transition zone and lengthen in convoluted, sinuous paths. As fingers lengthen, they may pinch off at their root near the original transition zone, or they may continue to grow. New fingers are continuously generated from the center of the cell in a region we call the "gradient zone." This zone slowly grows in time and for R_ρ=1.4, strong fingers always extend well outside. Often, new fingers that develop within the gradient zone become entrained within established older fingers. Once outside the gradient zone, adjacent fingers often merge, resulting in a preferred spacing between fingers greater than their spacing within the gradient zone. Repetition of entrainment and merger results in a series of conduits for upward and downward finger growth. Within a conduit, a stair step concentration field is evident as several fingers follow one another (Figure 3). With time, the gradient zone height increases and wider fingers develop within it. Thus longer, wider fingers form before becoming entrained, and subsequently merging outside of the gradient zone.

The evolving pattern of continuously developing and coalescing (merging) fingers progresses throughout the experiment as long as the criterion for instability is met. There is a very strong symmetry between the patterns that form in the upper and lower halves of the cell. The collective development of fingers seems to affect the largest-scale features; that is, in addition to their merging into conduits, these finger conduits shift laterally across the cell. Fingers eventually reach the upper and lower cell boundaries where they create layers of lower and higher density fluid, respectively.

The result is a greater density difference than at the start of the experiment; in time these regions at the extremities thicken vertically, mix with the fluid between the finger conduits, convect toward the center of the cell, and eventually feed the growing gradient zone. Thus, although the global fluid density gradient becomes steeper in time, the individual concentration gradients that drive the system within the finger gradient zone decrease, causing the eventual rundown of convection.

With increasing R_ρ, the development and structure of the unstable flow field slowly transitions as the diffusive and convective time scales converge. Fingers travel slower and somewhat straighter, and have larger diffuse regions around them than their lower R_ρ counterparts. Pinching off within the transition zone becomes less frequent at high R_ρ and fingers extend less far beyond the finger gradient zone. At R_ρ=2.8, initial fingers travel only ~1 to 2 cm before stalling and diffusing into the background. The new fingers that form still seem to follow the path of old fingers (as at lower R_ρ) and grow outward a bit further each time before stalling and diffusing. Thus, the solute mass remains closer to the original transition zone for higher R_ρ as fingers no longer extend beyond the gradient zone. Comparison of late-time images shown in Figure 2 shows wider and more diffuse features as R_ρ increases.

3.2 Structural Measures

Concentration fields can be integrated horizontally to give average concentration profiles. Figure 4 shows the profiles for the concentration fields shown in Figures 1 and 2. All the profiles are very symmetric about the center of the cell. For R_ρ=1.4 (Figure 4a) a clear characterization is seen of the gradient zone as the near-linear region between approximately 0.1 and 0.9. Outside of this zone the sharp change in slope depicts solute mass that is being transported out of the gradient zone by strong fingers into the tails of the profile. In Figure 4b, the profiles appear much more diffusive and lack the convective behavior in the tails as fingers do not grow outside of the gradient zone. A

diffusion solution with a diffusion coefficient 4×10^{-9} m^2 sec^{-1} is plotted for comparison. The choice of D is discussed in section 3.3.

Profiles for the late time fields (Figure 4c) show a much greater concentration spread about the center of the cell. For R_ρ=1.4 the near-linear profile through the center of the cell is confined to the distance encompassed by c/c_o between approximately 0.3 and 0.7. The concentrations nearly reach 0 and 1 at the top and bottom of the cell for R_ρ=2.4, as few fingers have reached the cell boundaries. For R_ρ=1.8 and 1.4, many fingers have reached the boundaries. For the R_ρ=1.4 experiment, the concentration profile has inverted near the top and bottom of the cell. Here, a significant number of fingers have reached the cell boundaries, and formed stable layers of more dense (bottom) and less dense (top) fluid. As mentioned above, this fluid mixes and is carried back toward the center of the cell between the convective finger conduits to eventually feed the gradient zone.

Figure 5 shows the growth in time of the gradient zone (h) for the four experiments. We define h operationally as the distance covered by one standard deviation of the c/c_o field above and below the horizontal centerline of the cell. The gradient zone grows nearly linear in time in the most unstable experiment, but as only $t^{1/2}$ in the more stable experiments (i.e., initial R_ρ of 2.4 and 2.8). These results are consistent with those of Taylor and Veronis (1996) who showed linear behavior with R_ρ<2.5 and $t^{1/2}$ behavior for larger values of R_ρ in laboratory tank experiments (i.e., non porous systems). Note that the break in slope at 800 minutes for R_ρ=1.4 is an artifact of our operable definition of the concentration defining the linear gradient zone. Beyond this time the concentrations defining the gradient zone has shortened beyond one standard deviation in c/c_o (e.g., see the profile for R_ρ=1.4 in Figure 4c).

Finger width at the location of the original transition zone is plotted as a function of time in Figure 6. Finger width was measured by counting the number of fingers across the cell and dividing by

this distance. The figure shows that for all four experiments, fingers widen in time as $\sim t^{1/2}$. At any given time, fingers are widest for the more unstable experiments and thinnest for the more stable experiments. However, experiments with the largest initial R_ρ eventually develop the widest fingers, which is consistent with arguments based on the buoyancy layer scale (L_o). The buoyancy layer scale is the horizontal distance over which concentration differences are adjusted across finger boundaries, and is therefore a scale pertinent to finite amplitude motion. The horizontal scales required for equilibrium fingers and those with maximum growth rates should be proportional to the buoyancy layer scale. For a Hele-Shaw cell, the buoyancy layer is (Veronis, 1987)

$$L_o = \left(\frac{\beta_1 \frac{dc_1}{dz} gk}{D_1 \nu} \right)^{-1/2} \tag{4}$$

where dc_1/dz is the vertical concentration gradient over the gradient zone, or h^{-1}. Smaller concentration differences result in wider fingers (larger L_o).

A "preferred scale," i.e., one that does not assume equilibrium (as does the buoyancy layer) but that does assume maximum finger growth rate and mass flux, is the maximum attainable wavenumber (Veronis, 1987; Shen and Veronis, 1991)

$$a_m = \left(\frac{1-(\tau R_\rho)^{1/2}}{1-\tau} \left[(\tau R_\rho)^{-1/2} - R_\rho^{-1} \right] \frac{\partial c_1}{\partial z} \right)^{1/2} . \tag{5}$$

In accordance with (5), the growth of finger width should scale with $h^{-1/2}\left(=\left[dc_1/dz\right]^{1/2}\right)$. Figure 7 shows the relationship between the dimensionless finger gradient zone height and dimensionless finger wavenumber (both nondimensionalized the buoyancy layer, L_o). The wavenumber, a [L^{-1}], is defined as $a = 2\pi/\lambda$ where λ[L] is the wavelength (or twice the finger width). In Figure 7, the correct 1/2 power law scaling is preserved; however, theory consistently underestimates the finger

wavenumbers by approximately an order of magnitude. This contrasts with Shen and Veronis' (1991) numerical simulations, which showed perfect agreement between the two for one experiment with an initial R_ρ of 1.5.

3.3 Mass transfer

Figure 8 shows the temporal change in mean c/c_o in the upper half of the cell for each experiment. Also shown are the times in which the first fingers reached the top and bottom of the cell. For R_ρ=1.4, the relationship is linear and remains so long after the first fingers have reached the upper and lower cell boundaries. The R_ρ=1.8 experiment shows linear behavior before, and for some time after (~600 minutes) the fingers reach the top and bottom of the cell. Beyond this time, the increase of mean concentration in the upper half of the cell slows. For the two experiments nearest stability (initial R_ρ=2.4 and 2.8), the time rate of change in concentration is very nearly $t^{1/2}$.

Figure 9 shows the temporal mass flux of dye across the centerline of the initial profile for each experiment. The mass flux was determined by first summing the mass associated with all pixels in the region and then forming a second order finite difference in time and dividing by the cross-sectional area of the cell.

The R_ρ=1.4 experiment shows very linear behavior in time. The R_ρ=1.8 experiment shows linear behavior prior to the fingers reaching the horizontal boundaries, and then decays after that time. Also plotted in Figure 9 is the one-dimensional solution for diffusive flux of dye for a step concentration initial condition. Mass flux of the most unstable experiment (R_ρ=1.4) is approximately one-and-a-half orders of magnitude greater than the flux predicted by the diffusion solution. For the most stable experiment (R_ρ=2.8), time-evolution of mass flux is bounded by the diffusion solution, under the same initial and boundary conditions. Taylor and Veronis (1996) saw similar results for experiments in ordinary fluids when R_ρ>2.5, i.e., square root of time behavior

and fluxes of order 10^{-6} kg m^{-2} sec^{-1}. The R_ρ=2.8 experiment was very nearly stable, although fingers in the experiment had most of the characteristics of fingers in more unstable experiments. This is a remarkable result, as even though the system was unstable and the patterns associated with transport were very different from those typically associated with molecular diffusion, temporal mass flux behaves in accordance with a diffusive model. Plotted in Figure 9 are diffusion solutions with effective diffusion coefficients that best fit the data of the R_ρ=2.4 and 2.8 experiments. The effective dispersion coefficients are 4×10^{-9} m^2 sec^{-1} and 10^{-8} m^2 sec^{-1}, respectively.

The data in Figure 9 are not as smooth the data in Figure 8 because those data show an accumulation of mass. The rich and complicated finger structure creates fluctuations in time and is emphasized by the differencing procedure in the flux plot, which offers little to smooth the data. Although the data for the most stable experiments are scattered, they approximate the trend predicted by a diffusive process.

4.0 SUMMARY AND CONDLUDING REMARKS

Double-diffusive fingers result when a transition layer containing two concentration profiles becomes unstable to perturbations. The resulting patterns of fluid motion are mm- to cm-scale fingers traveling upward and downward away from the transition layer, increasing their length and width scales in time. These two scales are balanced by the buoyancy layer, which is a horizontal boundary layer that adjusts lateral diffusion from the core of a finger to the vertical sodium chloride concentration gradient. In order for fingers to remain stable, they must widen as they lengthen. The buoyancy layer constantly adjusts to maintain this balance; the result is a smooth transition to wider, longer fingers in time.

Our experiments allow a detailed description of the dynamics of the evolving unstable flow field as a function of R_ρ. For low buoyancy ratio systems, fingers rapidly develop, merge with adjacent

fingers, form conduits, and stall before newer-generated fingers travel through the conduits and continue the process. Solute flux in low R_ρ systems quickly reaches steady state and is on the order of 10^{-6} m^2 sec^{-1}. For our R_ρ=1.4 experiment, the flux was one-and-a-half orders of magnitude greater than would be expected to occur in similar, though stable, diffusive systems. In the higher R_ρ experiments, fingers are slower to evolve and do not interact as dynamically as in the lower R_ρ systems. Our experiment with initial R_ρ=2.8 exhibited flux on the order of that expected for a similar diffusive system, although the structures were very different than the pattern of transport expected in a diffusing system. The temporal solute flux was also diffusive-like, as it decayed as $t^{1/2}$. Fingers widen in time as nearly $t^{1/2}$ in all of our experiments.

As in the experiments (Taylor and Veronis, 1986) and numerical simulations (Shen and Veronis, 1991; Stockman et al., 1998) in Hele-Shaw cells, and the experiments of Imhoff and Green (1988) in porous media, no large-scale circulation above or below the finger zone was seen. This suggests that large-scale circulation is a phenomenon in systems where friction due to viscosity does not play as great a role as it does in Hele-Shaw cells and porous media. This is a significant difference because in ordinary fluids (i.e., non porous media) large-scale circulation acts to limit the growth of fingers and set up the stair step pattern of groups of fingers that is seen in the ocean. In systems with negligible inertial forces, there is no understanding on the limits of growth, as models for salt fingers in ordinary fluids are not applicable to motion in isothermal (or low temperature gradient) porous media. The various "secondary" instabilities developed by Stern (1969, 1975), Holyer (1984), and Howard and Veronis (1987, 1992) which act to limit finger growth cannot exist in low Reynolds number systems. The implication to natural subsurface systems is that the upper bound on finger growth has not been reached for any value of R_ρ.

The degree to which fingers merge and create conduits for mass transport was limited by the size of the cell. A larger cell may have allowed fingers to continue merging laterally, creating larger and greater-spaced conduits for mass transport. Thus, in contrast to the small-scale buoyancy layer that

adjusts individual finger growth, the large horizontal length scale due to merging fingers has not been investigated. Its influence on large-scale transport is unclear.

No theory or experiments exist to understand the physics of finger growth and decay in heterogeneous and anisotropic porous media. Experiments in larger and heterogeneous systems are necessary in order to understand the phenomenon in even the smallest-scale natural subsurface systems. Nor are the effects due to different initial concentration profiles, influence of a third diffusing component, and chemical reactions in porous media understood as they undergone only limited investigation.

ACKNOWLEDGMENTS

Financial support for this research was provided by the U.S. Department of Energy's Basic Energy Sciences Geoscience Research Program under contract numbers DE-FG03-96ER14611 (Desert Research Institute) and DE-AC04-94AL85000 (Sandia National Laboratories). Experiments were conducted in the Flow Visualization and Processes Laboratories at Sandia National Laboratories. We thank Russ Detwiler for discussions on error within transmitted light systems, and Scott Pringle for constructive comments of the manuscript, and Brad Snyder for helpful discussions on stability theory.

REFERENCES

Bear, J., *Dynamics of Fluids in Porous Media*, 764 pp., Dover, New York, 1988.

Cooper, C.A., Glass, R.J., and S.W. Tyler, Experimental investigation of the stability boundary for double-diffusive finger convection in a Hele-Shaw cell, *Water Resour. Res.*, v. 33, 517-526, 1997.

Detwiler, R.L., Pringle, S.E., and R.J Glass, Measurement of fracture aperture fields using transmitted light: An evaluation of measurement errors and their influence on simulations of flow and transport through a single fracture, *Water Resour. Res.*, v. 35, 2605-2617, 1999.

Detwiler, R.L., H. Rajaram, and R.J. Glass, An investigation of the relative importance of Taylor dispersion and macrodispersion in variable aperture fractures, *Water Resources Research*, in press.

Green, T., Scales for double-diffusive fingering in porous media, *Water Resour. Res.*, v. 20, 1225-1229, 1984.

Griffiths, R.W., and B.R. Ruddick, Accurate fluxes across a salt-sugar finger interface deduced from direct density measurements, *J. Fluid Mech.*, v. 99, 85-95, 1980.

Holyer, J.Y., The stability of long, steady, two-dimensional salt fingers, *J. Fluid Mech.*, v. 147, 169-185, 1984.

Howard, L.N., and G. Veronis, The salt finger zone, *J. Fluid Mech.*, v. 183, 1-23, 1987.

Howard, L.N., and G. Veronis, Stability of salt fingers with negligible diffusivity, *J. Fluid Mech.*, v. 239, 511-522, 1992.

Imhoff, P.T., and T. Green, Experimental investigation of double-diffusive groundwater fingers, *J. Fluid Mech.*, v. 188, 363-382, 1988.

Lambert, R.B., and J.W. Demenkow, On the vertical transport due to fingers in double diffusive convection, *J. Fluid Mech.*, v. 54, 627-640, 1971.

Phillips, O.M., *Flow and Reactions in Permeable Rocks*, Cambridge, 285 pp., 1991.

Shen C.Y., and G. Veronis, Scale transition of double-diffusive finger cells, *Phys. Fluids*, v. 3, 58-68, 1991.

Stern, M.E., Collective instability of salt fingers, *J. Fluid Mech.*, v. 35, 209-218, 1969.

Stern, M.E., *Ocean Circulation Physics*, Academic, 1975.

Stern, M.E., and J.S. Turner, Salt fingers and convecting layers, *Deep-Sea Res.*, v. 16, pp. 497-511, 1969.

Stockman, H., Glass, R.J., Cooper, C.A., and H. Rajaram, Accuracy and computational efficiency in 3D dispersion via Lattice-Boltzmann: models for dispersion in rough fractures and double-diffusive fingering, *Int. J. Modern Phys. C*, v. 9, 1-13, 1998.

Taylor, J., Laboratory experiments on the formation of salt fingers after the decay of turbulence, *J. Geophys. Res.*, v. 96, C(7), pp. 12,497-12,510, 1991.

Taylor, J., and G. Veronis, Experiments on salt fingers in a Hele Shaw cell, *Science*, v. 231, 39-41, 1986.

Taylor, J., and Veronis, G., Experiments on double-diffusive sugar-salt fingers at high stability ratio, *J. Fluid Mech.*, v. 321, 315-333, 1996.

Turner, J.S., Salt fingers across a density interface, *Deep-Sea Res.*, v. 14, pp. 599-611, 1967.

Turner, J.S., *Buoyancy Effects in Fluids*, Cambridge, 368 pp., 1979.

Veronis, G., The role of the buoyancy layer in determining the structure of salt fingers, *J. Fluid Mech.*, v. 180, 327-342, 1987.

Figure 1. Evolution of the dye c/c_o field for experiments with R_ρ= 1.4 (a-c) and R_ρ=2.8 (d-f). The dye was dissolved in the sodium chloride solution. Images were chosen such that equivalent global (i.e., effective) concentrations in the upper and lower halves of the cell could be compared. The mean c/c_o of (a) and (d) is 0.018, (b) and (e) is 0.036, and (c) and (f) is 0.054. The times since the start of each experiment are (a-c) 52, 177, and 304 minutes; (d-f) 370, 2752, and 6871 minutes. The black line across the center of cell shows the location of the slot in the cell where the plastic slider was removed to begin the experiment.

Figure 2. Comparison of images for the mean c/c_o=0.10 field in half of the cell for the R_ρ=1.4, R_ρ=1.8, and R_ρ=2.4 experiments. The times are 320, 1085, and 3398 minutes, respectively. The dye was dissolved in the sucrose for the R_ρ=2.4 experiment and was dissolved in the sodium chloride for the other two experiments.

Figure 3. Normalized concentration profile (c/c_o; dye dissolved in the sodium chloride) of an individual finger with several follower fingers. The finger (a) shows the stair step pattern represented by the leader finger with individual followers; the corresponding concentration profile along the axis of the finger is shown in (b).

Figure 4. Horizontally averaged c/c_o across the cell when the mean global concentration field in the upper (lower) half of the cell is (a) 0.018, (b) 0.054, (c) and 0.1. Shown in (b) is an error function solution to transient diffusion in an infinite half space with D=1.59 × 10^{-9} m^2 sec^{-1} and t=250 minutes. The data support a model that transport for high R_ρ systems is diffusive-like.

Figure 5. Growth of the finger gradient zone (h) defined by the distance encompassed by ±1 standard deviation of the horizontally averaged NaCl concentration field as in Figure 4. Also shown are $t^{1/2}$ curves to show that transport agrees with diffusive behavior for the R_ρ=2.8 experiment, but is slightly faster for the R_ρ=2.4 experiment. For the R_ρ=1.4 and 1.8 experiments,

measurement of the zone became vague, as upward traveling fingers met the oppositely moving advective mass to create a large vertical zone of nearly constant concentration. Therefore, not all of the late time data are plotted. The X marks the time at which the fingers reached the cell boundary in each experiment. Fingers never reached either horizontal boundary in the R_ρ=2.8 experiment.

Figure 6. Growth of finger widths showing that merging, branching, and dissipation act collectively to produce a smooth, coherent scale change. The most stable experiments have the widest fingers; if the R_ρ=2.8 experiment had been allowed to run past 20,000 minutes, it would possibly have had fingers wider than those in the R_ρ=2.4 experiment. The solid $t^{1/2}$ curve shows that in general, fingers widen as $t^{1/2}$.

Figure 7. The 1/2 power law relationship between finger zone height and wavenumber. Finger widths, however, are approximately one order of magnitude less than those predicted by theory (5).

Figure 8. Evolution in time of the mean c/c_o in half of the Hele-Shaw cell. The dye was dissolved in the sucrose for the R_ρ=2.4 experiment and sodium chloride for the other three experiments. The X marks the time at which the fingers reached the cell boundary in each experiment. Fingers never reached either horizontal boundary in the R_ρ=2.8 experiment. Also plotted are square root of time curves, showing the relationship of the R_ρ=2.4 and 2.8 to theoretically diffusive behavior.

Figure 9. Fluxes of dye (i.e., mean c/c_o) in time for all four experiments. The dye was dissolved in the sucrose for the R_ρ=2.4 experiment and sodium chloride for the other three experiments. Solid lines are one-dimensional solutions to the diffusion equation for similar initial and boundary conditions with varying diffusion coefficients. Although fingering is advective, for the two highest R_ρ experiments, data can be fitted with a diffusion solution with an effective dispersion coefficient.

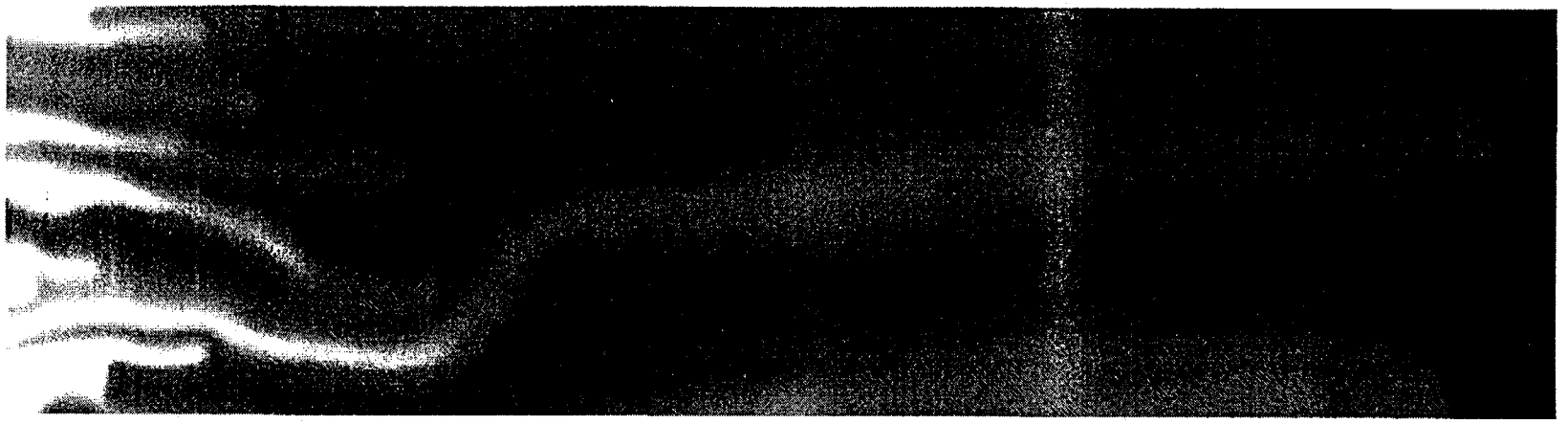

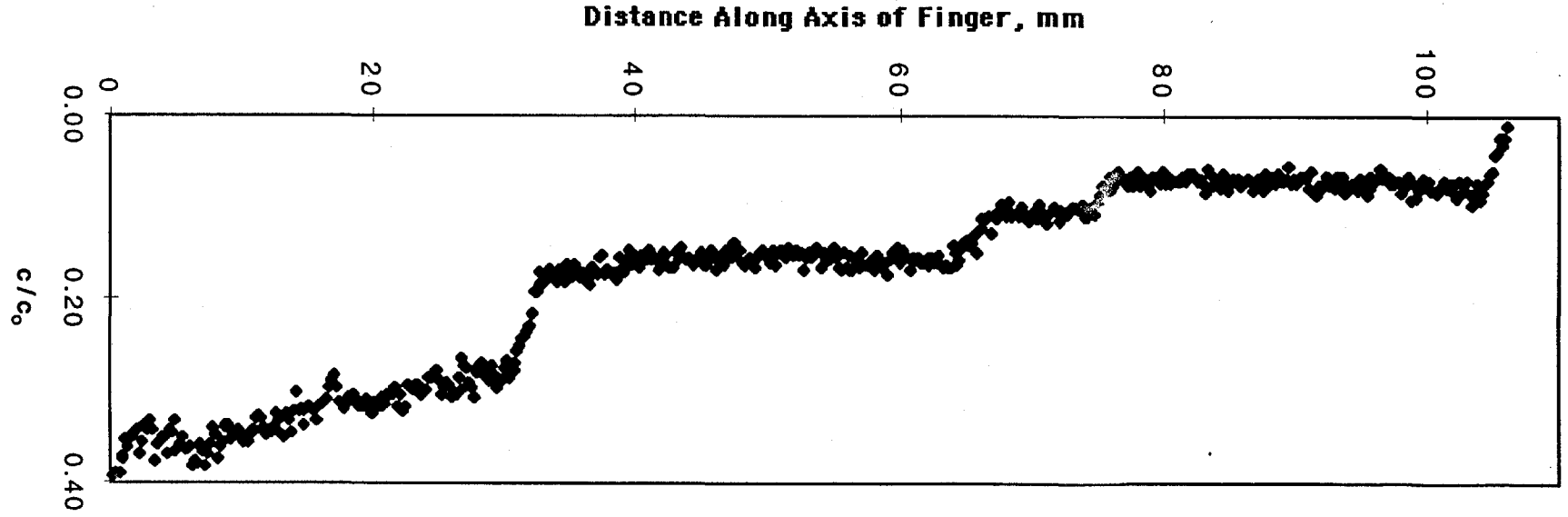
Distance Along Axis of Finger, mm
0
20
40
60
80
100
0.00
0.20
0.40
c/c0

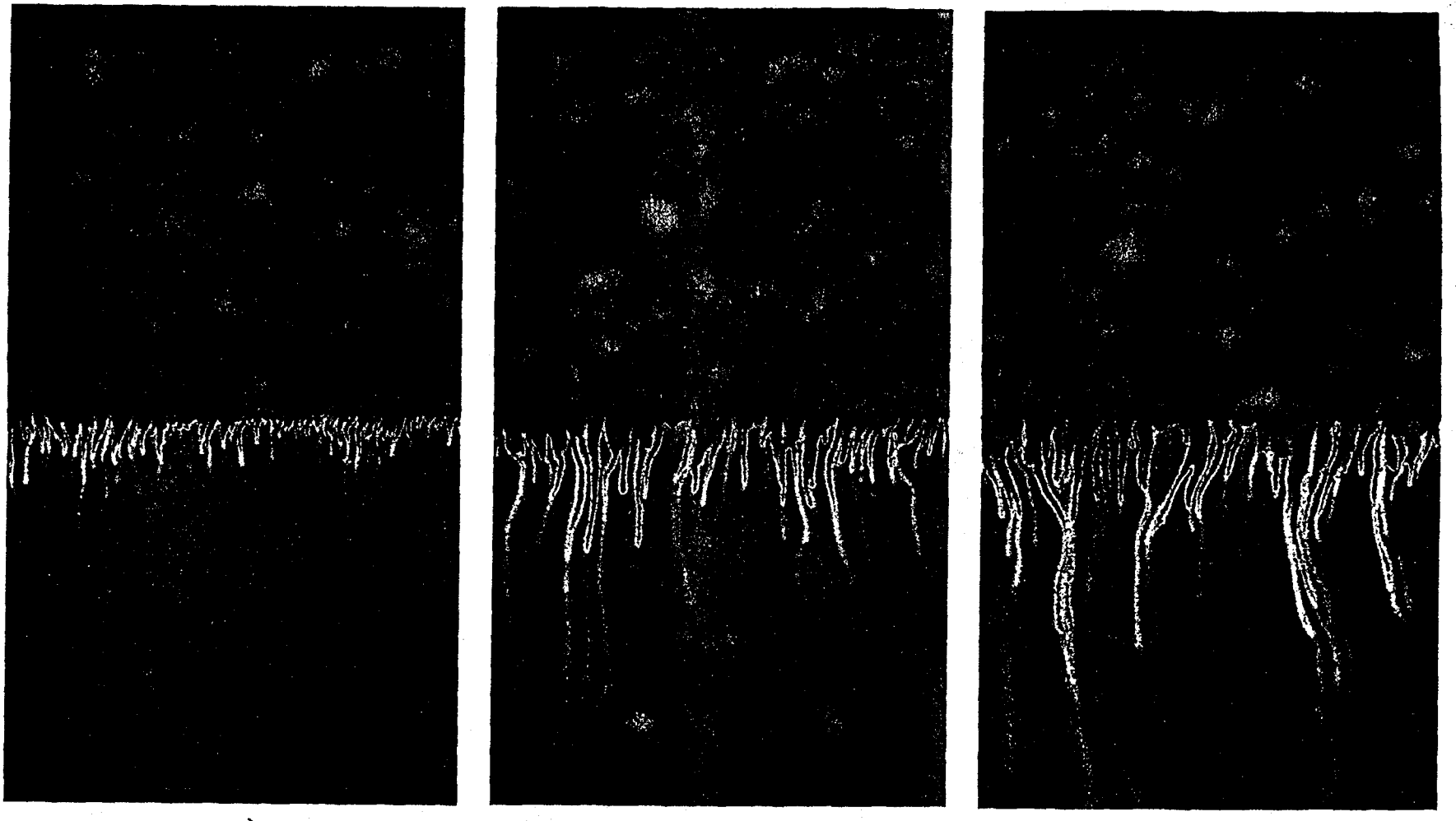

Figure 1

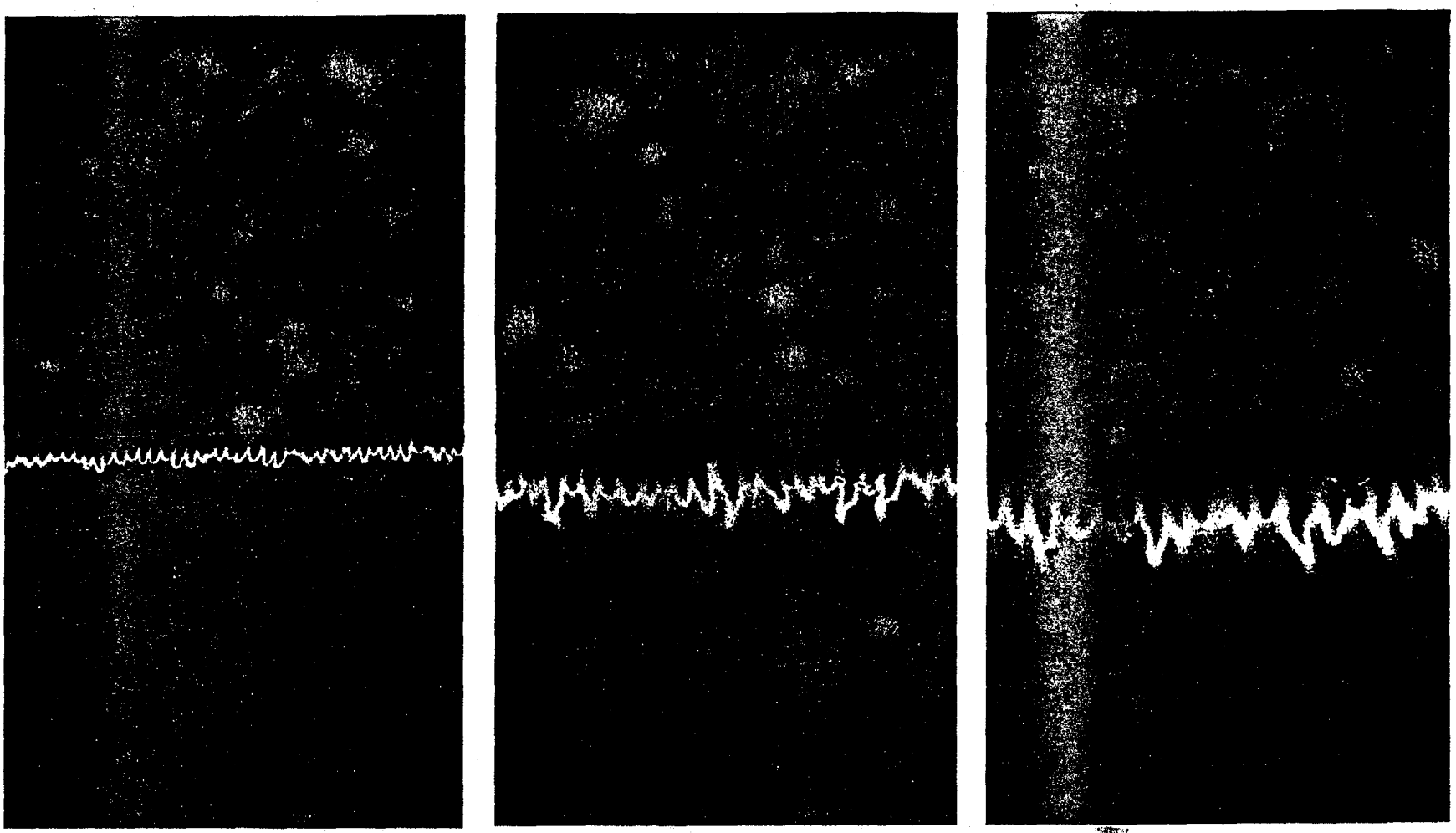

d) e) f)

0 1

c/co

Figure 1 continued

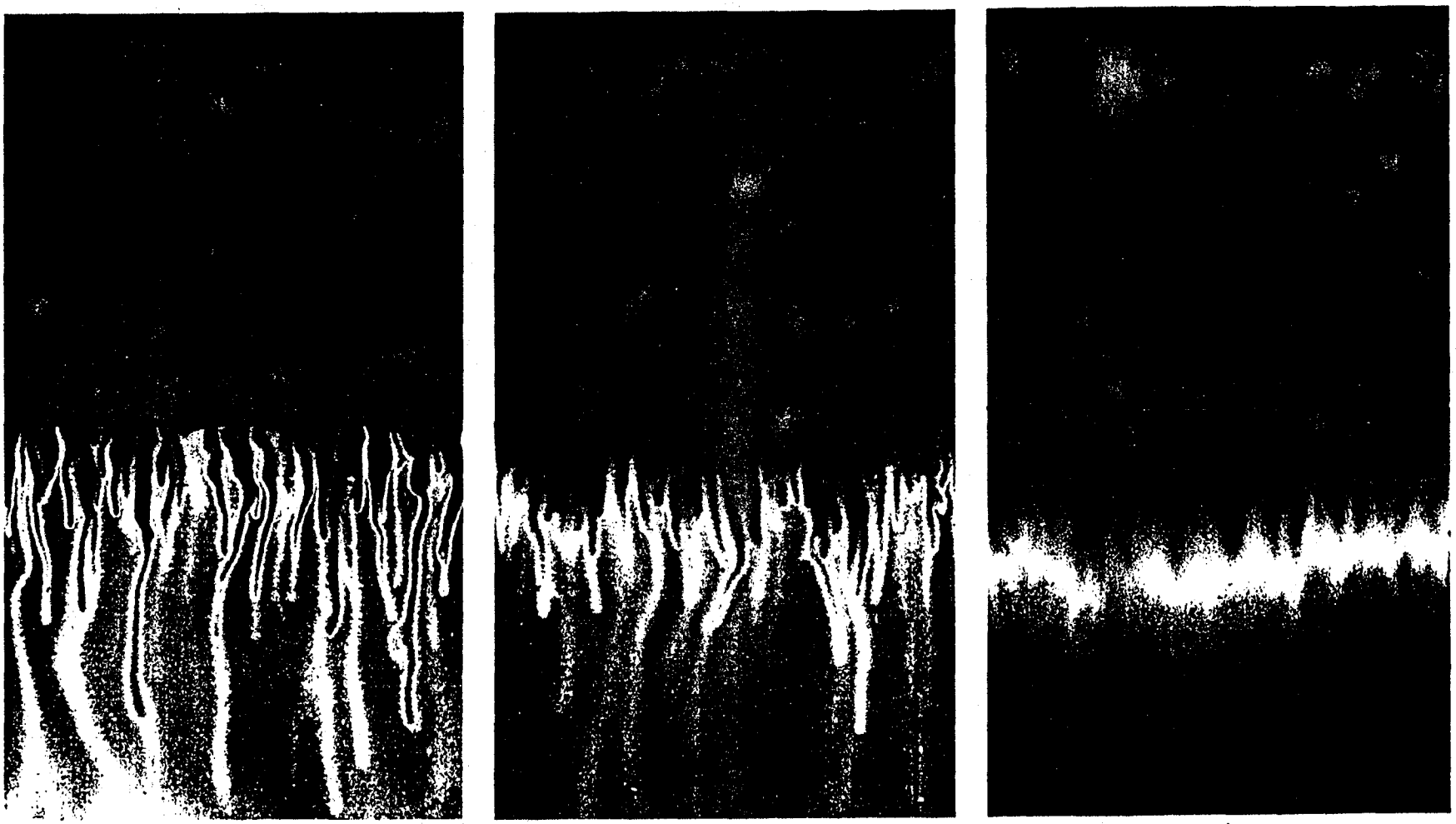

Figure 2

Fig. 4a

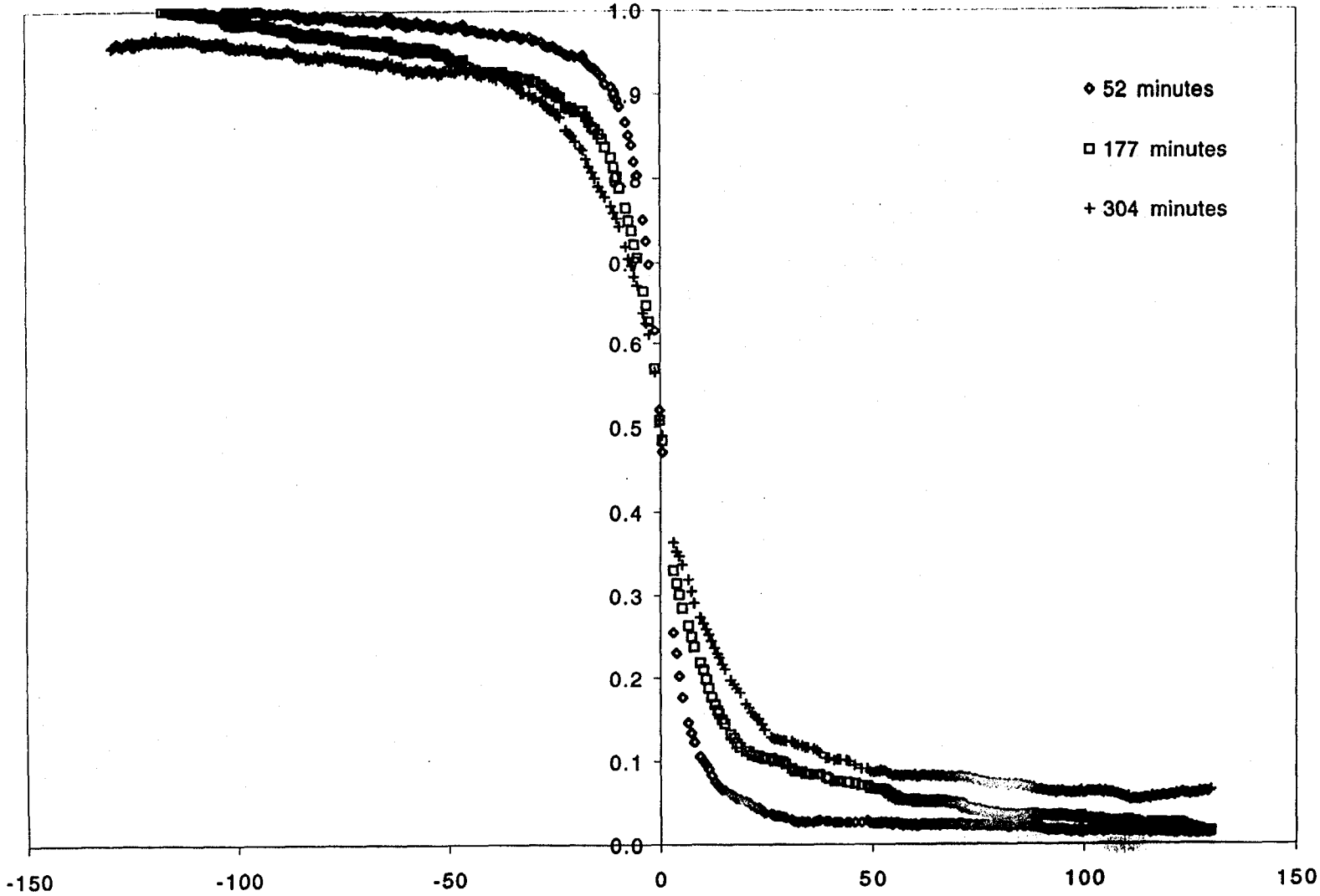
1.0
0.9
0.8
0.7
0.6
0.5
0.4
0.3
0.2
0.1
0.0
-150
-100
-50
0
50
100
150
52 minutes
177 minutes
304 minutes

Fig 4b

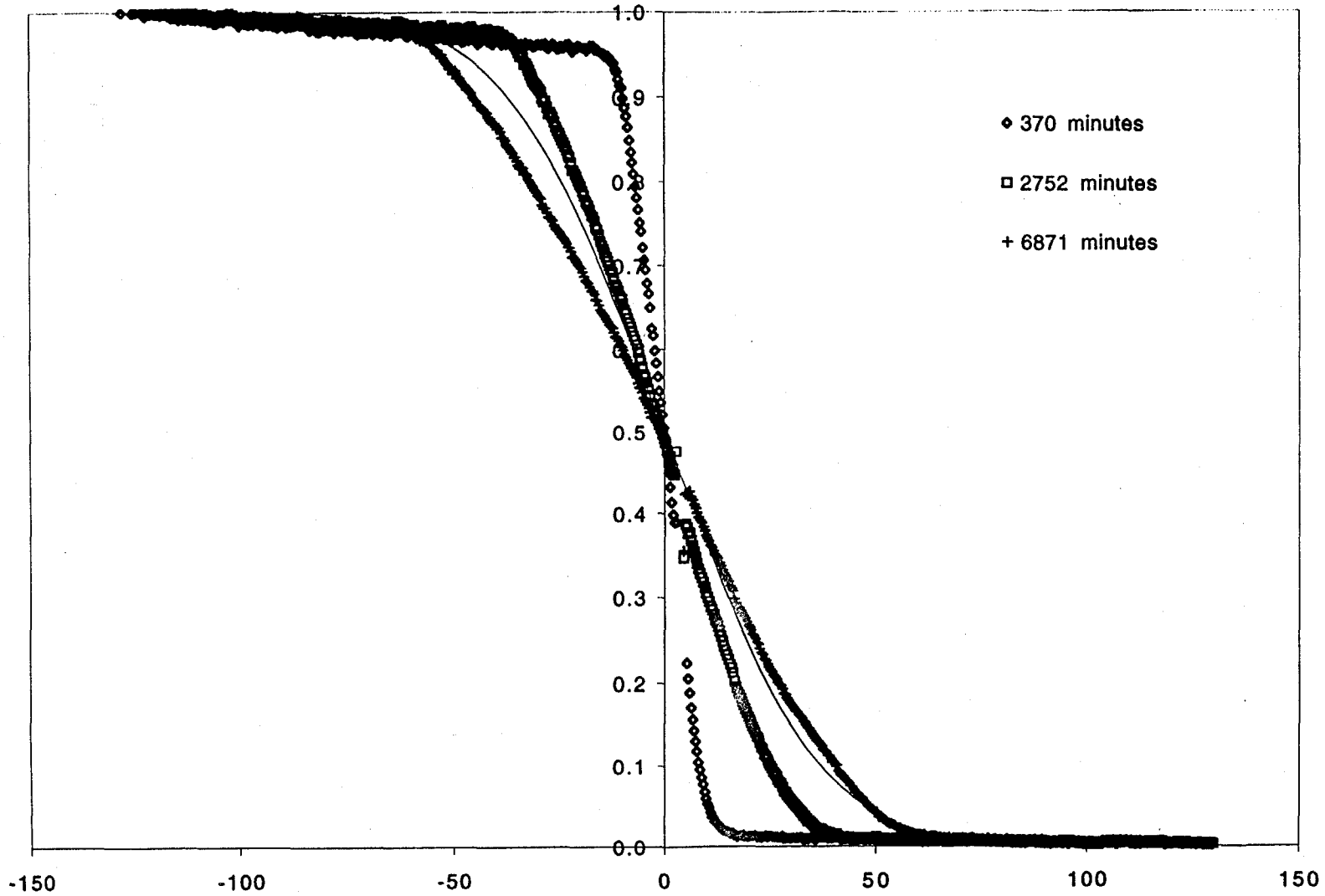
1.0
0.9
0.8
0.7
0.6
0.5
0.4
0.3
0.2
0.1
0.0
-150
-100
-50
0
50
100
150
370 minutes
2752 minutes
6871 minutes

Fig 4c

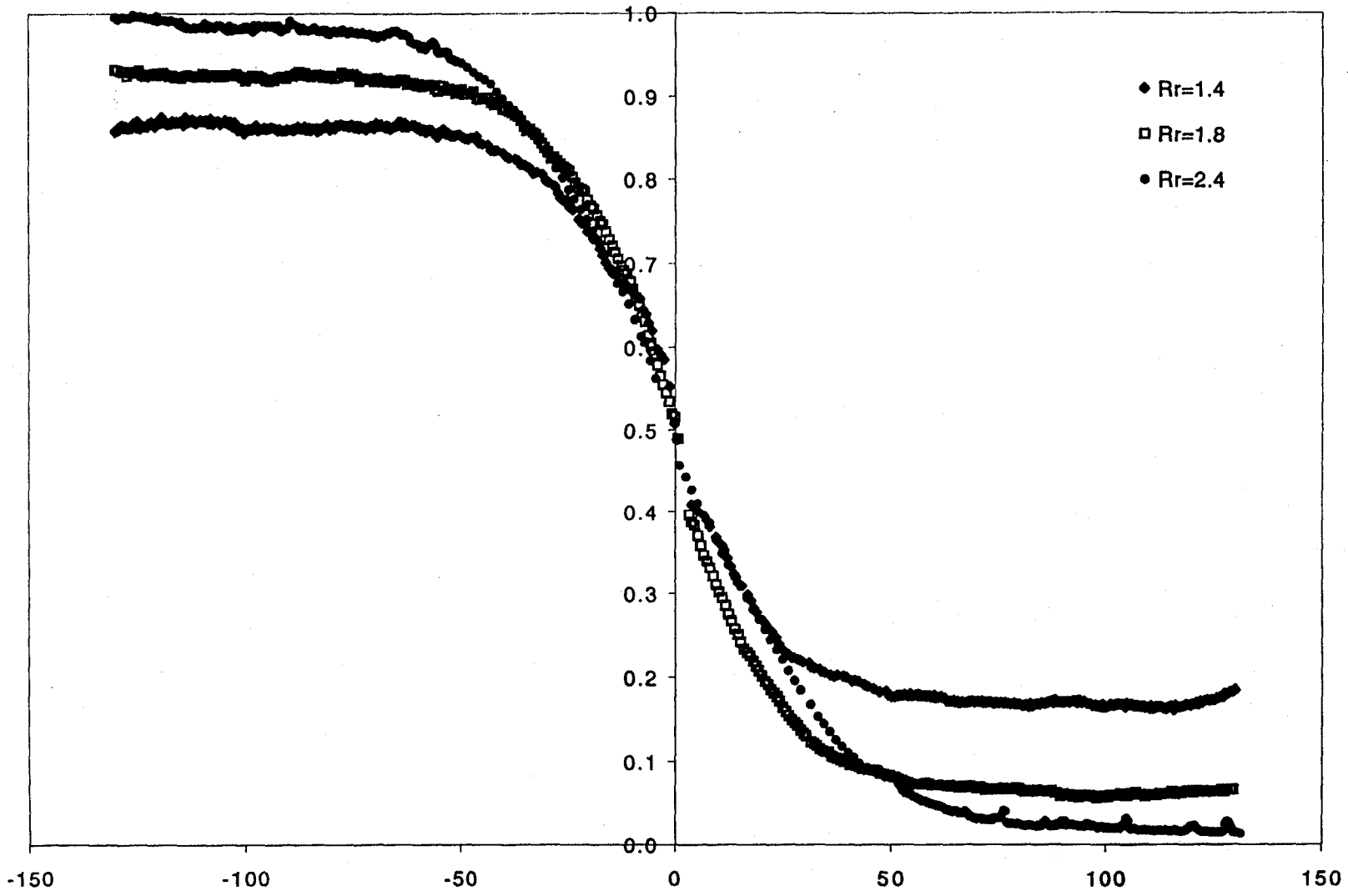

Fig 5

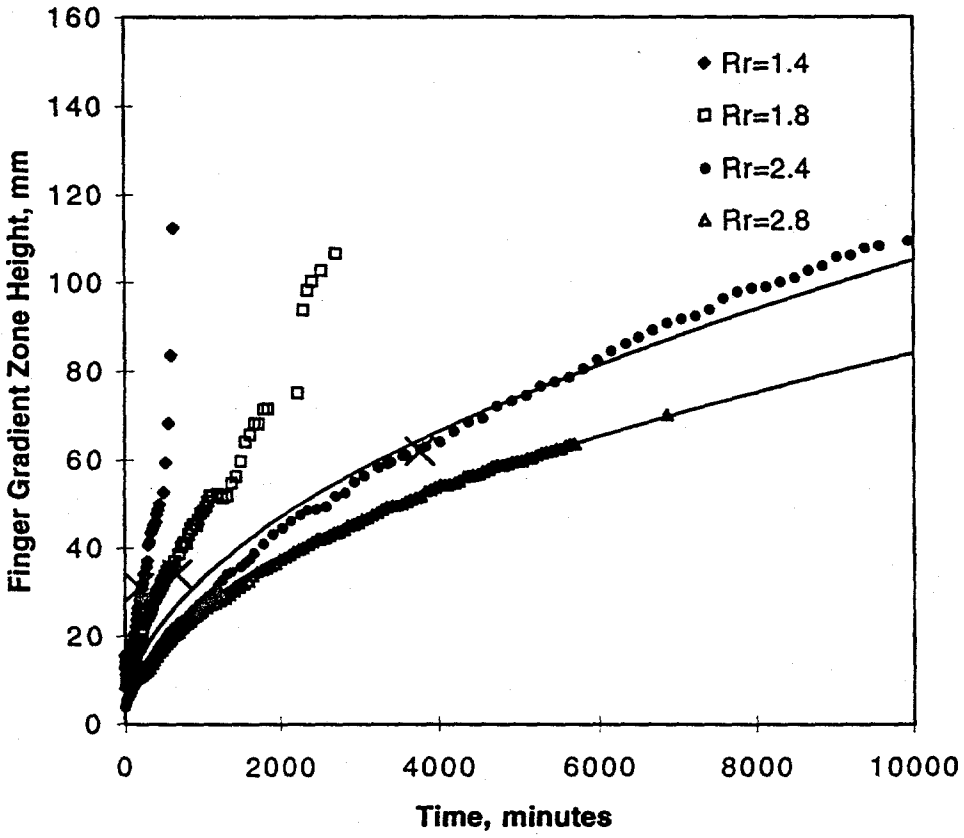
Finger Gradient Zone Height, mm
Time, minutes
Rr=1.4
Rr=1.8
Rr=2.4
Rr=2.8
0
20
40
60
80
100
120
140
160
0
2000
4000
6000
8000
10000

Fig 6

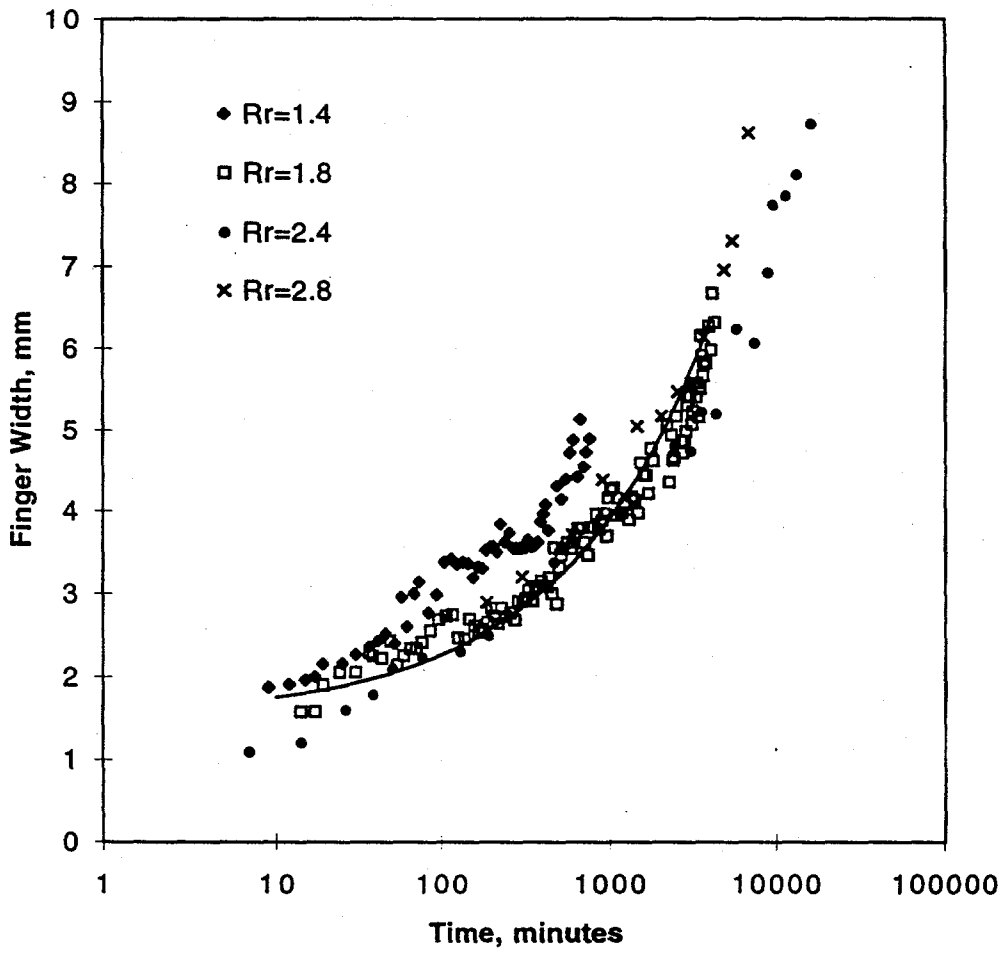
Rr=1.4
Rr=1.8
Rr=2.4
Rr=2.8
Finger Width, mm
Time, minutes
0
1
2
3
4
5
6
7
8
9
10
1
10
100
1000
10000
100000

Fig 1

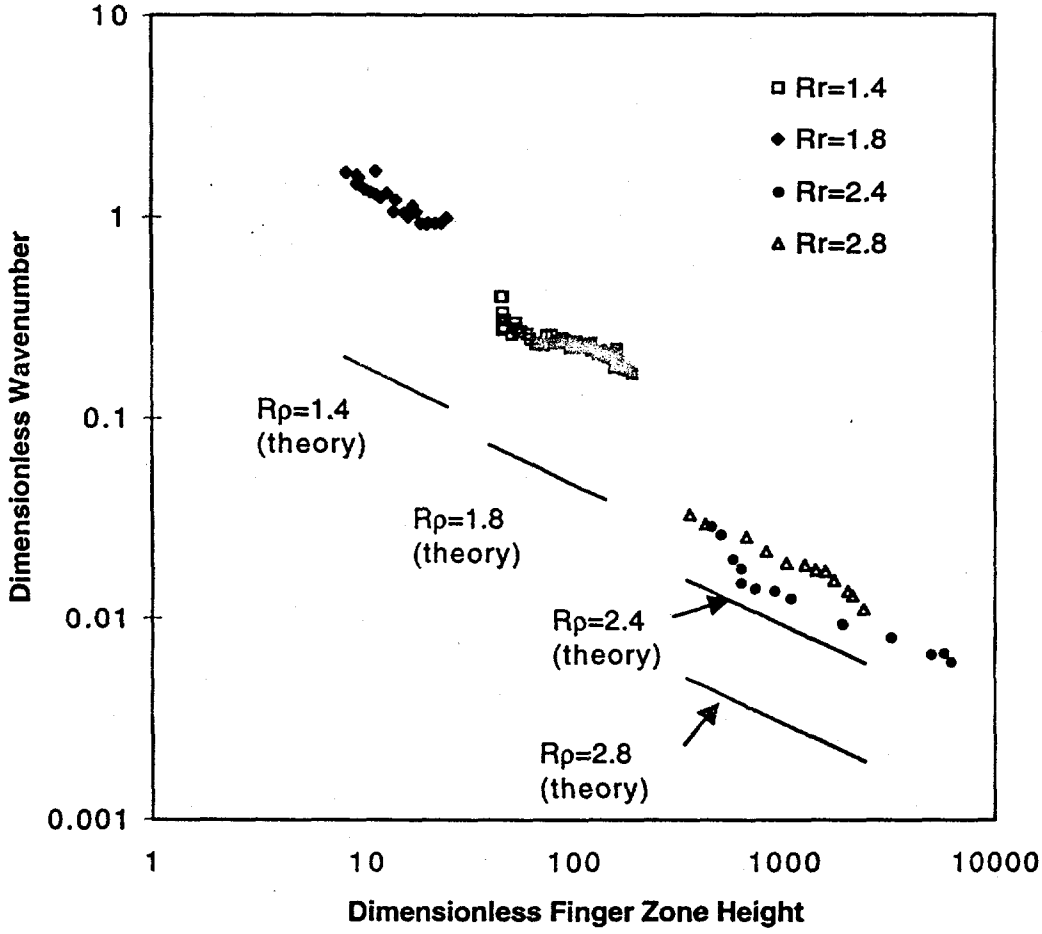
10
1
0.1
0.01
0.001
1
10
100
1000
10000
Dimensionless Wavenumber
Dimensionless Finger Zone Height
Rr=1.4
Rr=1.8
Rr=2.4
Rr=2.8
Rρ=1.4
(theory)
Rρ=1.8
(theory)
Rρ=2.4
(theory)
Rρ=2.8
(theory)

fig 8

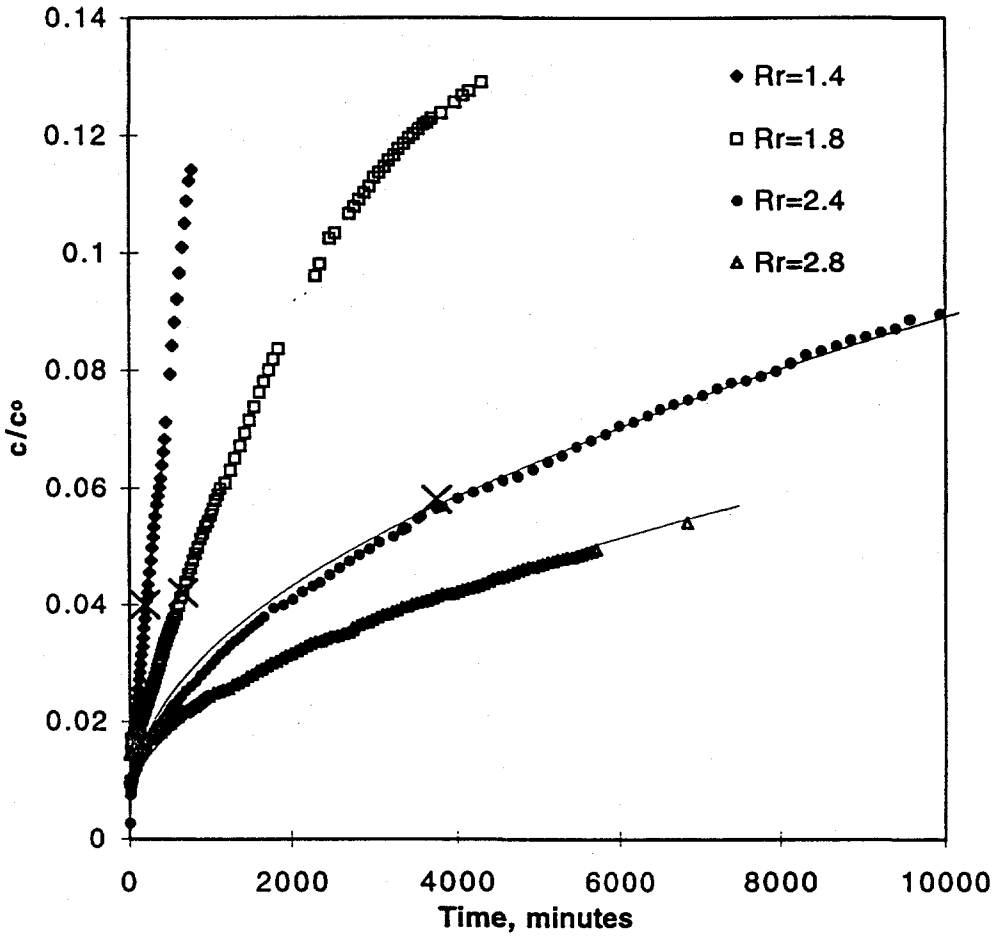
0.14
0.12
0.1
0.08
0.06
0.04
0.02
0
c/co
0
2000
4000
6000
8000
10000
Time, minutes
Rr=1.4
Rr=1.8
Rr=2.4
Rr=2.8

Fig 9

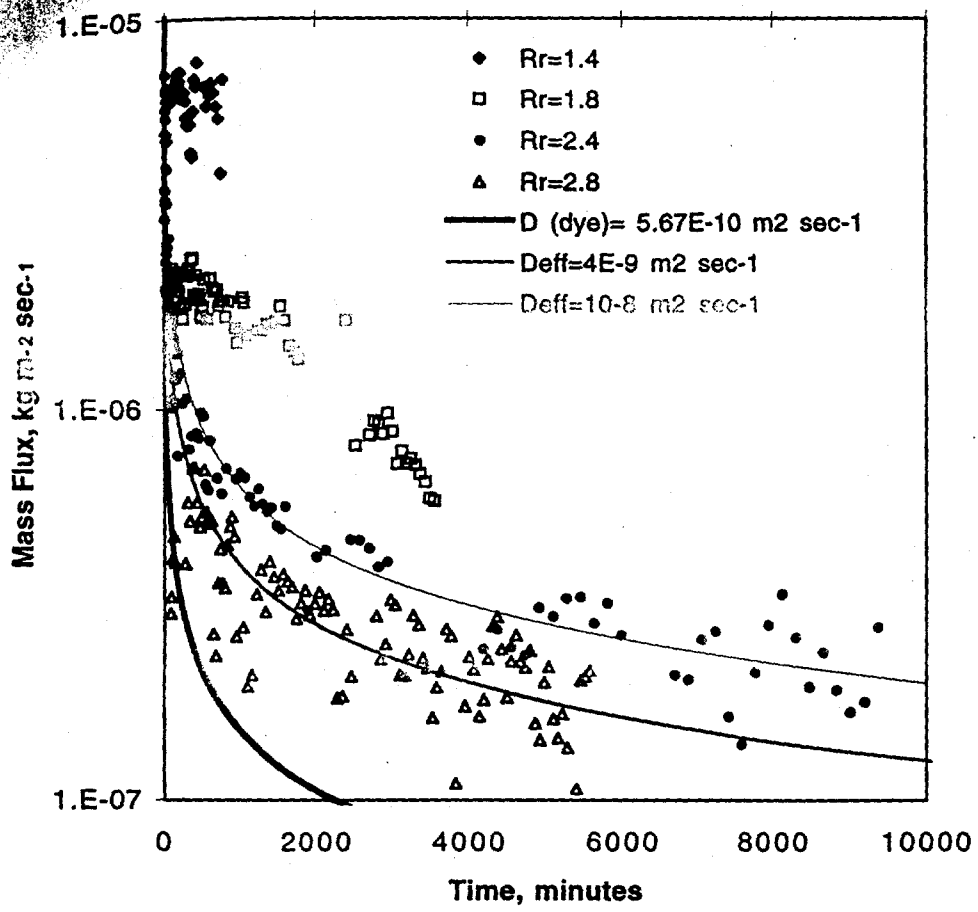
1.E-05
1.E-06
1.E-07
Mass Flux, kg m-2 sec-1
0
2000
4000
6000
8000
10000
Time, minutes
Rr=1.4
Rr=1.8
Rr=2.4
Rr=2.8
D (dye)= 5.67E-10 m2 sec-1
Deff=4E-9 m2 sec-1
Deff=10-8 m2 sec-1